International Journal of Mass Spectrometry 478 (2022) 116875

Contents lists available at ScienceDirect

International Journal of Mass Spectrometry

journal homepage: www.elsevier.com/locate/ijms

The gas phase reaction of iridium and iridium carbide anions with 2-hydoxyethylhydrazine (HEH)

Moritz Blankenhorn [a], Tatsuya Chiba [a], Jerry A. Boatz [b, **], Steven D. Chambreau [c, ***], Gerd Ganteför [d], Kit H. Bowen [a, *]

[a] Department of Chemistry, Johns Hopkins University, Baltimore, MD, 21218, USA
[b] Propellants Branch, Rocket Propulsion Division, Aerospace Systems Directorate, Air Force Research Laboratory, AFRL/RQRP, Edwards Air Force Base, California, 93524, United States
[c] Jacobs Technology, Inc., Air Force Research Laboratory, AFRL/RQRP, Edwards Air Force Base, CA, 93524, United States
[d] Department of Physics, University of Konstanz, Konstanz, 78457, Germany

ARTICLE INFO

Article history:
Received 14 April 2022
Received in revised form
13 May 2022
Accepted 18 May 2022
Available online 21 May 2022

Keywords:
2-hydoxyethylhydrazine (HEH)
Iridium
Iridium carbide
Monopropellant
Photoelectron spectroscopy
Density functional theory

ABSTRACT

Understanding the chemistry of compounds that are similar to hydrazine has two advantages. First, it helps to identify less hazardous propellants to replace hydrazine as the most widely used monopropellant. And second, it helps to gain insight into the reaction mechanism that could be analogous to the decomposition of hydrazine into ammonia and nitrogen. Ionic liquids have already shown to be promising candidates to replace hydrazine. The molecule investigated in this study is 2-hydroxyethlyhydrazine ($HOCH_2CH_2NHNH_2$; HEH), which is a neutral precursor to the ionic liquid 2-hydroxyethylhydrazinium nitrate (HEHN) and differs from hydrazine by the substitution of a hydrogen with a hydroxyethyl group. Gas phase photoelectron spectroscopy and density functional theory were used to examine the reaction between a HEH molecule and an Ir^- anion as well as with IrC^-. Suggested by the experimental and theoretical data, Ir^- and IrC^- react with HEH and can attack the C—N, C—O, N—N, C—H and the C—C bond in HEH.

1. Introduction

Despite its high toxicity, hydrazine has been commonly used as a monopropellant, where the fuel is ignited over a catalyst bed. To improve safety and make handling easier, hydrazine-based ionic liquids have attracted attention as a replacement. Ionic liquids (melting point must be below 100 °C) have negligible vapor pressure, which means they can be handled with lower risk of human exposure. Ionic liquids to be used as monopropellants in a thruster should ignite without an external ignition source on a catalyst, thereby reducing the complexity of the thruster design, as the ionic liquid only needs to be sprayed onto the catalyst. Hydrazine and its derivatives for example have this property [1]. Hydroxylammonium nitrate (HAN) is an example of an ionic liquid that has already shown improvements in safety and efficiency over hydrazine as a monopropellant [2–4]. 2-hydroxyethylhydrazine (HEH)-based ionic liquids are also attractive candidates. Shamshina et al. showed that 2-hydroxyethylhydrazinium nitrate (HEHN) and 2-hydroxyethylhydrazinium dinitrate (HEH2N) ignite when in contact with an alumina-supported iridium catalyst [1]. Other ionic forms of HEH have also been invented for monopropellant applications such as the chloride and dichloride salts [5].

Out of many hydrazine-based ionic liquids that have been studied, HEHN has a significant advantage. While most of the other potential ionic liquid candidates are solids at room temperature, HEHN is liquid (glass transition at −56.9 °C [1]), making it possible to handle in fuel lines and to introduce onto the catalyst. HEHN also has higher thermal stability compared to other ionic liquids used as propellants [1], and is more stable than HEH, making it preferable for practical use.

While HEHN is an ionic liquid consisting of protonated HEH (HEH-H^+, $HOCH_2CH_2N^+H_2NH_2$) and NO_3^-, the first step of the HEHN decomposition is proton transfer to NO_3^- to form neutral HEH and nitric acid [6,7]. Zeng et al. also showed, via cryogenic vibrational

* Corresponding author.
** Corresponding author.
*** Corresponding author.
E-mail addresses: jerry.boatz@us.af.mil (J.A. Boatz), steven.chambreau.ctr@us.af.mil (S.D. Chambreau), kbowen@jhu.edu (K.H. Bowen).

https://doi.org/10.1016/j.ijms.2022.116875
1387-3806/

spectroscopy, that the HEHN ion-pair has neutral characteristics and can be treated as a HEH-HNO_3 complex [8]. The less well understood step of the mechanism is the further decomposition of HEH by a catalyst, which is investigated in this study.

Iridium is used as a catalyst in thrusters to decompose hydrazine, HAN or HEHN. Like other elements in the platinum group, iridium and its derivatives are used commonly as a catalyst in a wide variety of reactions [9–13]. Additionally, iridium and its complexes have been shown to activate a variety of molecules [14–16]. Hydrazine for example is activated by iridium (I) complexes, and the N–H bond is cleaved in the reaction [17]. Cleavage of the N–H bond was also observed for the hydroxylamine-iridium reaction [18]. Although a great amount of research has already been done to characterize hydrazine decomposition on iridium, no consensus on the catalytic mechanism has been established yet [19–21].

To imitate the active site in catalysts, single metal atoms can often be used as a good model [22–26]. Using those single metal atoms gives insight into the different steps that are happening on a molecular level between the catalysts and the reactant, for example breaking and forming bonds [27–33].

In this study, a combined theoretical and experimental approach was used to investigate the mechanism of the catalytic process. On the experimental side, a combination of time-of-flight mass spectrometry and photoelectron spectroscopy were utilized. On the theoretical side, density functional theory (DFT) was used to predict the probable products, followed by simulations of the corresponding photoelectron spectra. These combined methods have shown that Ir^- as well as IrC^- can attack the carbon atoms in the HEH molecule and they can break the N–N, the N–C, the C–O, the C–C as well as every kind of C–H and N–H bond. These findings line up with previous experiments by Esparza et al. and Howard et al. that showed that in the thermal decomposition of HEH, a large number of different compounds formed, including ethanolamine, ammonia and hydrazine [34,35]. This indicates the breaking of several different bonds in the HEH molecule, including for example the C–N bond to form hydrazine.

2. Methods

2.1. Experimental details

Anions were generated using a laser vaporization-reaction cell arrangement described previously [18] and described briefly here. A rotating and translating iridium rod was ablated by the 2nd harmonic of Nd:YAG laser (532 nm, 2.33 eV), and helium backing gas delivered the iridium products through a nozzle into the reaction cell, where the iridium beam was crossed with a gaseous HEH and helium mixture. The resulting particles were introduced into the time-of-flight mass spectrometer through a skimmer. Anions were then mass-selected by accelerating them in a Wiley-McLaren type time-of-flight mass spectrometer, and photodetached by crossing the ion beam with a laser, after decelerating the anions. The kinetic energy of the photodetached electrons was measured by a magnetic bottle electron energy analyzer to obtain photoelectron spectra.

The detachment process is governed by the energy-conservation relationship: $h\nu$ = EBE + EKE, where $h\nu$ is the energy of the photon, EBE is the electron binding energy, and EKE is the kinetic energy of the photodetached electron. From this relationship the binding energy can be obtained by measuring the kinetic energy of electrons photodetached by a Nd:YAG laser operating at 3rd harmonic (355 nm, 3.49 eV). The energy resolution of the magnetic bottle is ~35 meV at EKE = 1 eV [36]. The photoelectron spectra were calibrated by the well-known transitions of Cu^- atomic anions [37].

2.2. Theoretical details

The structures and relative energies of several isomers and electronic spin states of $[Ir–N/C/O/H]^-$ anionic species corresponding to the *m/z* fragments detected experimentally were calculated using density functional theory (DFT) methods, with the objective of identifying the most stable species, for which the electronic vertical detachment energies (VDEs), adiabatic detachment energies (ADEs), and photoelectron spectra (PES) were subsequently computed. The ωB97x-d [38,39] range-separated functional, which includes dispersion corrections, in combination with the def2-TZVPPD basis set [40,41] for all atoms and the Stuttgart quasi-relativistic pseudopotential [42,43] for iridium were used [44–46]. This pairing of functional and basis set, hereafter denoted simply as ωB97x-d/def2, was shown in a recent study [18] to be a suitable computational approach for a similar series of $[Ir–N/O/H]^-$ anions. All structures were fully optimized and confirmed as local minima via diagonalization of the mass-weighted matrix of energy second derivatives with respect to nuclear coordinates, i.e., the Hessian matrix. Relative Gibbs free energies at 298.15 K were calculated at all stationary points, with thermal and entropic corrections obtained from standard rigid-rotor, harmonic oscillator approximations [47], using harmonic vibrational frequencies scaled by a factor of 0.975 [48]. Restricted and unrestricted DFT calculations were performed for closed- and open-shell systems, respectively. All electronic structure calculations were performed using the GAMESS quantum chemistry program. [49,50].

Photoelectron spectra were computed using the ezFCF program suite developed by Gozem, Wojcik, Mozhayskiy, and Krylov [51,52], utilizing the double harmonic approximation with Franck-Condon factors obtained using Duschinsky rotations [53]. The full set of 3N–6 (3N-5 for linear species) vibrational modes, where N is the number of atoms, were included in the calculations. The simulated photoelectron spectra were obtained using the following protocol:

(i) Sufficient vibrational quanta V_f were included in the target (neutral) state to generate initial state (anion) → target state (neutral) energy transitions up to 3.5 eV, the highest energy measured in the experiments.
(ii) Using a Boltzmann temperature of 300 K to estimate thermal populations of vibrational hot bands in the initial (anion) state, the number of vibrational quanta V_i in the initial state was systematically increased until the simulated spectra showed no significant changes.
(iii) Final PES simulations were generated using the thus-determined values of V_i, V_f, and a Boltzmann temperature of 300 K.

3. Results and discussion

The results, obtained from the mass and the photoelectron spectra, supported by the calculations, indicate that there were two different interactions occurring. The first is the interaction of Ir^- with HEH, and the second is the interaction of IrC^- with HEH. The source of carbon to form IrC^- is most likely from the steel housing of the laser vaporization source. The carbide then forms with Ir in the helium stream. Therefore, IrC^- is already present in the beam before it crosses the HEH and helium beam in the reaction cell. This is a known behavior for Ir formed in the used source. It was observed in experiments with the laser vaporization source and iridium in previous experiments (for example in the reaction of Ir^- with hydroxylamine [18]). Attempts to suppress the IrC^- formation

were unable to eliminate it completely. However, the formation of IrC^- before the actual interaction with the HEH gives the opportunity to look at the reaction of IrC^- and HEH as well.

In the mass spectra in Fig. 1, five main peak series can be identified, the series of the elemental iridium (consisting out of the two isomers with an abundance of 37% for ^{191}Ir and 63% for ^{193}Ir) and four others. Two additional series can be found at higher masses, but their intensities are very low, and will not be discussed here.

Depending on the source conditions, the intensity of the IrC^- peaks changed. Fig. 2 shows the mass spectra for different IrC^- concentrations. It can be observed that some of the peaks have different intensities while others have similar intensities, potentially indicating reaction products from a $IrC^- + HEH$ reaction. Both spectra are normalized to the iridium peak at $m/z = 193$, so the reaction products from the reaction of iridium with HEH should have similar intensities in both mass spectra. There are similarities in the intensities in the peak distributions in series 2, 3 and 5 in Fig. 2, but the peak intensities differ dramatically in series 4 that are likely reaction products from reactions of IrC^- and HEH. Different source conditions could of course also just lead to iridium anions in different electronically excited states, leading to different reaction products. But for example, different laser powers alone will give different amounts of carbon from the housing of the laser vaporization source. Masses in series 4 could correspond to formation of $IrC_3H_x^-$ species, but there is no source for the third carbon atom in the reaction of Ir^- and HEH. The possible existence of this species could be explained by IrC^- reacting with HEH to provide the third carbon atom. The existence of $IrC_3H_x^-$ product ions will be discussed below.

Additionally, the lowest mass detected in series 5 is shifted for the different concentrations of IrC^- present; With a high concentration of IrC^- in the beam (red trace in Fig. 2), series 5 starts at $m/z = 241$ ($^{191}IrC_3N^-$). Having a low concentration of IrC^-, series 5 starts at $m/z = 245$ ($^{191}IrNC_2O^-$). This can be explained by the fact that HEH has only two carbon atoms, needing an extra carbon from the IrC^- to form IrC_3X^- species, indicating that both Ir^- and IrC^- are reacting with HEH in these experiments.

Looking at the entire mass spectrum in Fig. 1, almost all the HEH was fractured by the Ir^- or IrC^- upon exposure to the anion beam,

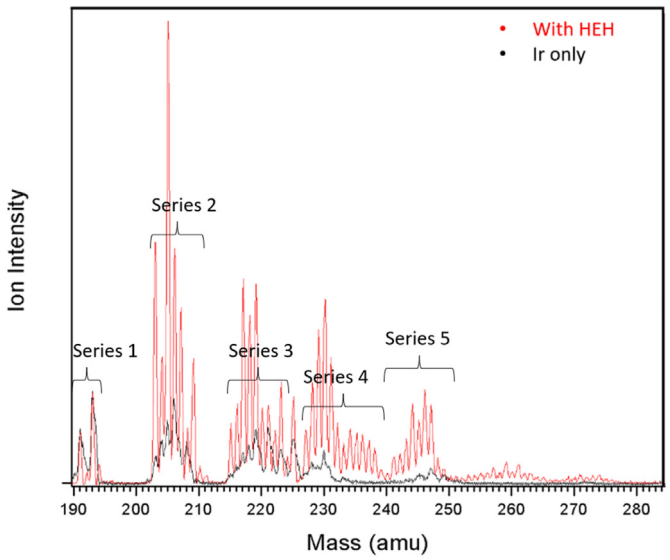

Fig. 1. Mass spectrum of iridium anions, with the addition of HEH (red) and the pure Ir^- spectrum in black. Both spectra are normalized to the ^{193}Ir peak. Smaller peaks in the black spectrum might be from residual HEH in the interaction region or the pulsed valve.

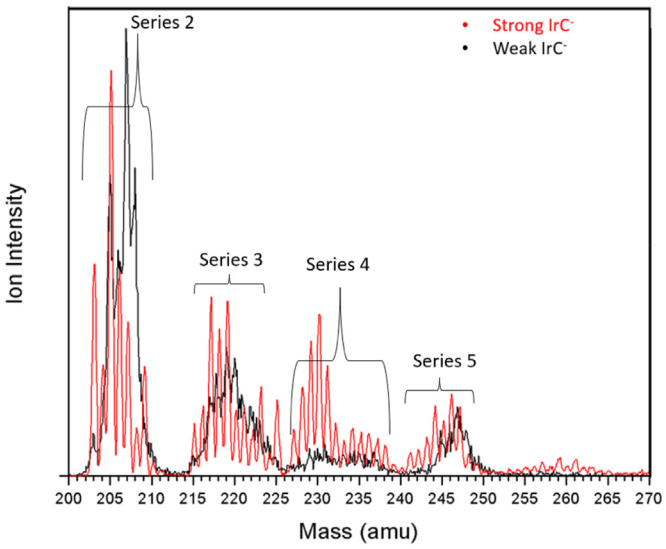

Fig. 2. Mass spectra from the Ir^- and HEH reaction for different source settings, with a high abundance of IrC^- (red) and with a low abundance of IrC^- (black). Both spectra are normalized to the ^{193}Ir peak (not shown).

indicating a complex reaction mechanism, as there was little to no intact HEH molecules observed attached to Ir^- or IrC^- or by itself in the mass spectrum (at $m/z = 265$ or 267 and 277 or 279). This fact already eliminates the possibility of a simple physisorption between the iridium species and HEH. The large differences in the photoelectron spectra compared to the well-known iridium atomic anion spectrum [18] additionally indicate that a chemical reaction is occurring.

Because of the atomic complexity of HEH (C, N, O, H) and the isotopic pattern of iridium (of 63% 193 and 37% 191), there can be multiple different possible products contributing to each mass peak, especially as product mass increases. In order to find out which species contribute to the peaks at the different masses and to investigate if series 4 contains $IrC_3H_x^-$ species, photoelectron spectra were taken and compared to the theoretically predicted PE spectra. Interest was paid mostly to the masses with the highest intensities in each series, assuming those would be the most prevalent products. A summary of all found reaction pathways can be found in Figs. 8 and S14.

3.1. Analysis of the photoelectron spectra

The masses $m/z = 203$, 205 and 207 (series 2) are in the first series of peaks after the elemental iridium peaks. Their high intensities in the mass spectra indicate that those might be the main reaction products. The photoelectron spectra of $m/z = 205$ and 207 were taken, as seen in Figs. S1 and 3a.

Looking at all atoms that are present in the reaction, IrC^- is the only plausible species that shows up in the $m/z = 205$ spectrum but not in the $m/z = 207$ spectrum. The subtraction of the $m/z = 207$ spectrum from the $m/z = 205$ spectrum should thereby yield the spectrum of IrC^- which is the green feature in Fig. 3b. The spectrum of $m/z = 207$ is shown in 3a and the spectrum for $m/z = 205$ in Fig. S1 can be found in the supporting information. Comparing the spectra to the theoretical data in Fig. 3 shows a reasonable match between experimental and simulated results (Electron affinity (EA), theoretical: 2.0 eV and experimental: 2.4 eV). Another theoretical value for the EA found in the literature matches within 0.2 eV (2.20 eV) [54] and calculations at the coupled cluster level predict an EA of 2.36 eV (see Table S1.) The theoretical values for IrN^-

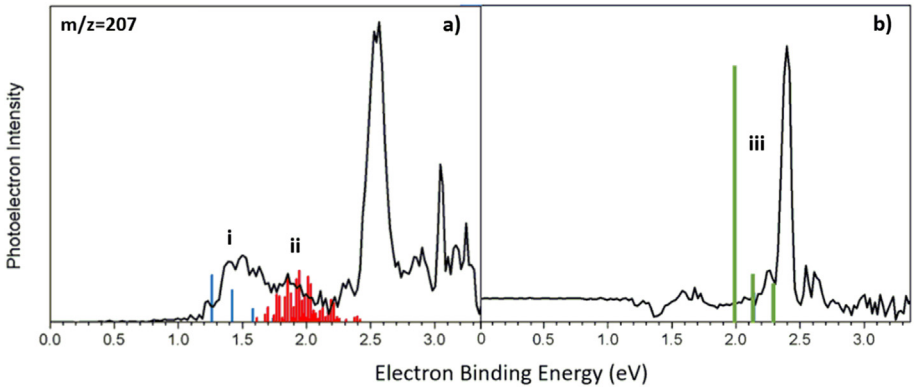

Fig. 3. Photoelectron spectra of a) $m/z = 207$ and b) the difference spectrum from $m/z = 205$ and $m/z = 207$. The theoretical calculated features of **i** IrN^- (blue), **ii** $IrCH_2^-$ (red) and **iii** IrC^- (green) are added to the spectra. The calculated structures of $IrCH_2^-$ and $IrCH_2$ are shown in Fig. S2.

correspond to a feature between 1.2 and 1.7 eV and the theoretical values from $IrCH_2^-$ correspond to a feature between 1.7 and 2.2 eV. The fact that the mass spectrum shows a significant increase of $m/z = 203$ and 205 species between the Ir^- only spectrum and the $Ir^- + HEH$ spectrum in Fig. 1, indicates that IrC^- is likely a product of the reaction between Ir^- and HEH. For species at $m/z = 207$, from the photoelectron spectrum it is difficult to differentiate which one of IrN^- and $IrCH_2^-$ is the main product. However, in the mass spectrum (Fig. 1), the IrC^- peaks seem to increase more with the addition of HEH than the $IrN^-/IrCH_2^-$ peaks.

Series 3 begins with $m/z = 215$, most likely being IrC_2^-. The species with $m/z = 218$, containing the heavier iridium species, and thereby having the higher intensity, is most likely $^{193}IrC_2H^-$ because species containing only one carbon, one oxygen or a nitrogen would contain high amounts of hydrogen. It would contain at least nine hydrogens (for $^{193}IrOH_9$), while HEH itself only has eight hydrogens. That means even for $IrOH_9^-$ an additional interaction between Ir^- and a second HEH molecule would need to occur to gain more hydrogen, which is unlikely in this experimental setup. Minding the low pressure in the source chamber (around 5×10^{-5} Torr in the source chamber, mean free path ≈ 6 cm), every additional collision makes a reaction pathway less likely. Additionally, only a small amount of HEH will be in the He that is introduced through the pulsed valve, meaning only the smallest part of the interactions will be between Ir^- and HEH. This is the case even when the pressure inside of the reaction cell is much higher than the rest of the chamber when the pulsed valve is open. Because of the low probability of multi collision interactions the focus was laid on products of a reaction between one Ir^- anion with one HEH molecule.

The other plausible species at $m/z = 218$, coming from a $Ir^- + HEH$ reaction, is $^{191}IrNCH^-$. The PE spectra of both species are shown in Fig. 4. DFT calculations show that the lowest energy structure for IrC_2H^- has two additional isomers close in energy (see Fig. S4.) Similarly, the calculations predict three isomers of $IrNCH^-$ with similar low energies, but only the most stable of these, included in Fig. 4, has a predicted VDE within the relevant energy range (see Fig. S5.) The three isomers of IrC_2H^- can be seen in Fig. 4, together with their theoretical spectrum, and the theoretical spectrum of $IrNCH^-$. The most likely way to form IrC_2H^- is by either Ir^- cleaving the N—C bond, leaving the C—C bond intact, or by IrC^- cleaving the C—C bond. The parent anion Ir^- or IrC^- would then only be bonded to part of the HEH molecule and additionally lose hydrogen atoms. $IrNCH^-$ forms in a similar way, by cleaving other bonds, likely the N—N bond. However, because of the similarities in the PE spectrum of $IrNCH^-$ and one of the isomers of IrC_2H^-, no

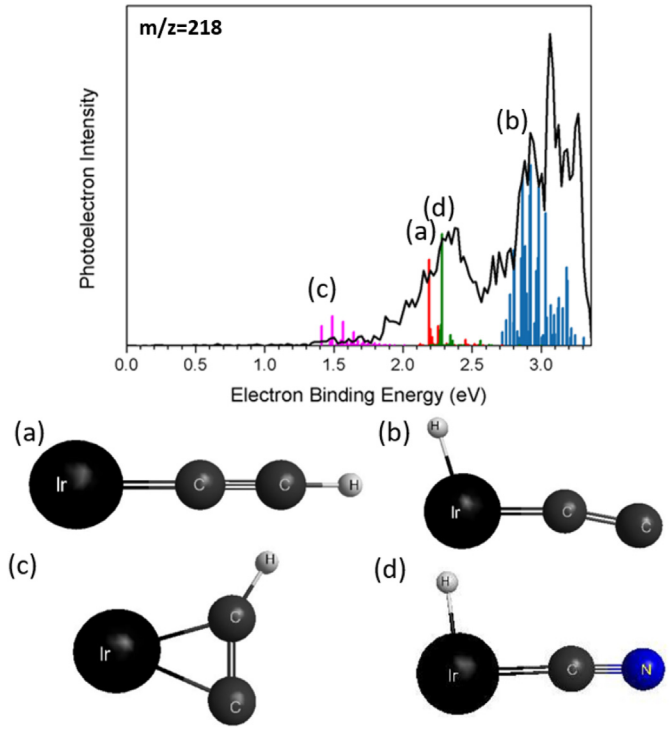

Fig. 4. Photoelectron spectrum of the $m/z = 218$ species. Additionally, the theoretical values for three $^{193}IrC_2H^-$ isomers (with the relative Gibbs free energy a) $\Delta G_{rel} = 0$ kJ/mol, b) $\Delta G_{rel} = 90$ kJ/mol and c) $\Delta G_{rel} = 91$ kJ/mol) and $^{191}IrNCH^-$ were added. $^{191}IrC_2H_3^-$ did not have a spectrum due to poor Franck Condon overlap between anion and neutral (see Fig. S3 in the supporting information).

final conclusion about the N—N bond can be made. These multistep, complex reaction mechanisms are still the most likely ones (similar to what was observed in the reaction of iridium clusters and hydroxylamine) [18], because a different reaction mechanism would include HEH reacting with Ir^-, breaking apart, and then having the fragments of HEH reacting with other HEH molecules or reaction products. This would include multiple interactions between different particles, which is less likely to occur in the vacuum environment.

Looking at isomer a) and b) of IrC_2H^- in Fig. 4, it seems that the Ir^- cleaved a C—H or the C—N in a) and the C—H bond in b). Additionally, all the C—H, the C—O and the C—N (if it was not cleaved) bonds were broken. The breaking of all these bonds must have been

caused by the interaction with the iridium anion because HEH under vacuum conditions and at room temperature is rather stable. In isomer c) the iridium atom is directly bonded to two different carbon atoms. This could be due to the Ir^- cleaving the C—N bond, a C—H bond or binding to both carbon atoms in HEH, leaving C_2H bond to the iridium while dropping the rest of the HEH molecule, or IrC^- cleaving the C—C bond or a C—H bond leaving CH with the IrC^-. These are both plausible but since there is no significant change in the intensities for this series for different amounts of IrC^-, making them more likely a product of the Ir^- with HEH reaction.

Possible reactivity of IrC^- with HEH can be seen by looking at the $m/z = 230$ and 231 species, because they are most likely IrC_3H^- and $IrC_3H_2^-$. As discussed previously for Fig. 2, the theoretical data compared to the PES in Fig. 5 implies that the species at $m/z = 230$ is $^{193}IrC_3H^-$ and at $m/z = 231$ is $^{193}IrC_3H_2^-$, while other species with the same mass also might be present in the PE spectra. The reason that both peaks are present in both spectra is limited mass resolution ($m/\Delta m \approx 400$) of the experiment. Even though they are resolved in the mass spectra (Fig. 1), and the species were mass-separated with a mass gate having a width of around 2 amu, the species still overlap to some extent in the photoelectron spectrum. This happens in most of the obtained spectra, because of the sheer number of different species in this experiment, giving every species a direct left and right neighbor (with 1 amu difference). Despite this limitation, the theoretical VDE values of 2.0 and 3.4 eV see Table S1) for the two species line up closely with the two main peaks in the spectra at 2.2 and 3.3 eV. As shown in Table S1, wavefunction-based calculations at the MP2/def2-TZVPPD level predict a VDE of 2.1 eV for IrC_3H^-, in good agreement with the DFT result and the lower experimental peak at 2.2 eV. However, the MP2/def2-TZVPPD predicted VDE value of 4.1 eV for $IrC_3H_2^-$ does not agree well with either the DFT prediction or the higher experimental peak at 3.3 eV (See Figs. S6 and S7 for the calculated isomers and relative free energies of IrC_3H^- and $IrC_3H_2^-$, respectively.). The possible formation of IrC_3H^- and $IrC_3H_2^-$ both indicate that IrC^- could react with HEH, resulting in attachment of C_2H_x ($x = 1,2$) to IrC^-. The observed vertical detachment energy (VDE) of $IrC_3H_2^-$ is higher than IrC_3H^- by ~1.1 eV, which is perhaps due to the additional H directly bonded to the iridium. There is a much smaller concentration of IrC_2^- ($m/z = 215,217$) in the reacting beam compared to IrC^- ($m/z = 203,205$ see Fig. 1, Ir only), making it less likely that the $IrC_3H_x^-$ forms from a reaction of IrC_2^- with HEH. The predicted shapes of the $IrC_3H_x^-$ products with one carbon on one side of the iridium atom and the other carbons on the opposite side of Ir, also supports the idea that $IrC_3H_x^-$ is formed by reaction of $IrC^- + HEH$.

All the obtained spectra so far have shown either Ir^- or IrC^- attaching to a carbon atom of HEH. As mentioned before there are five main series in the mass spectrum in Fig. 1. The first series consists of the elemental Ir^- with its isotope pattern of 63% ^{193}Ir and 37% ^{191}Ir. The second series starts with a mass of $m/z = 203$, $^{191}IrC^-$ and progresses to $IrCH_2^-$. The third series starts at $m/z = 215$, indicating $^{191}IrC_2^-$, and then progresses to IrC_2H^- and up to $IrC_2H_5^-$ ($m/z = 222$). The two peaks at $m/z = 223$, 225 likely have contributions from IrO_2^-. The fourth series starts at $m/z = 227$ with $^{191}IrC_3^-$. The photoelectron spectra of the species with $m/z = 230$ and 231 show that the series contains further hydrogenated species of IrC_3^-. Other species such as IrC_2N^- might also contribute to the PES of the $m/z = 231$ spectrum, but the two main peaks in Fig. 5 are assigned to the theoretical values of the carbon species (IrC_3H^- and $IrC_3H_2^-$, Table S1).

To see if the higher masses in series 4 came from the limited dehydrogenation of the $IrC_3H_x^-$ species, the photoelectron spectrum of $m/z = 236$ was taken. For $m/z = 236$, a possible molecule would be $IrC_2NH_5^-$, although its simulated photoelectron spectrum did not show any peak in the calculated energy range from 0 to 3.5 eV. This is due to poor Franck-Condon overlap between the anionic and neutral species, caused by the significant increase in the C—Ir—C bond angle as shown in Fig. 6. This large change in the geometry of the molecule will give a poor Franck-Condon overlap between the anionic and the neutral state and thereby a predicted spectrum that is zero over the whole energy range. The fact that there was still an experimentally obtained spectrum means that there is another species with the same mass, such as $IrCN_2H_3^-$ or $IrC_3H_7^-$. Some of the features in the spectrum might be explained by the presence of $IrC_3H_7^-$ (Figs. S8 and S9), while $IrCN_2H_3^-$ (Fig. S10) shows poor Frank Condon overlap between neutral and anion (geometrical structures are shown in Fig. S43). This indicates that series 4 consists, at least partly, of IrC_3H_x species.

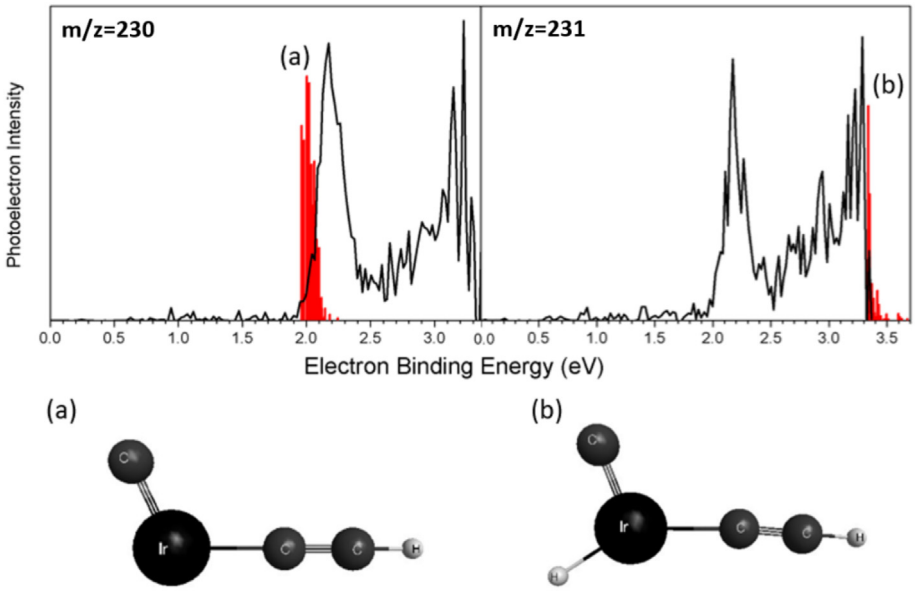

Fig. 5. Photoelectron spectra of $m/z = 230$ and 231, with the theoretical features from a) $^{193}IrC_3H^-$ in the left spectrum and b) from $^{193}IrC_3H_2^-$ in the right spectrum, both in red. Both peaks show up in both spectra because of limited mass separation.

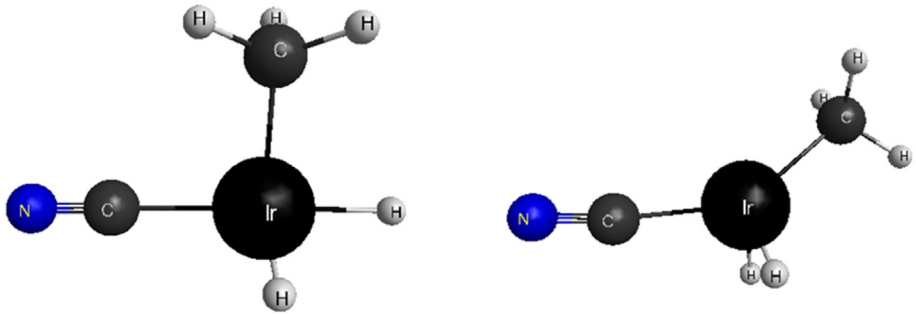

Fig. 6. Lowest energy theoretical structure of $IrC_2NH_5^-$ as an anion (left) and a neutral (right). The removal of an electron from the anion increases the C–Ir–C bond angle.

The next question is regarding the source of series 5, starting at $m/z = 241$. Another addition of carbon is unlikely, thereby ruling out $IrC_4H_X^-$. Starting at $m/z = 241$, IrC_3N^- has the right mass. The theoretical data suggests that breaking of the N–N bond is the most energetically efficient way of attacking HEH by iridium or iridium carbide (see Table S2, NH_3 elimination).

To pursue this, photoelectron spectra of the masses 245 and 247 were measured (Fig. 7).

As shown in Table S1, the calculated electron affinities of the lowest energy isomers of species $IrNC_2O^-$ (Fig. S11) and $IrC_2N_2H_2^-$ (Fig. S12) are 3.51 eV and 4.61, respectively, which are beyond the energy limit of photodetachment in our experimental setup. Although the leading edge of the VDE peak of $IrNC_2O^-$ should show up in the high energy limit of the spectrum, in order to detect the formation of $IrNC_2O^-$ in the ion beam a different experimental setup with a higher photon energy would be needed. But there are additional peaks in this spectrum (Fig. 7), which could be from $IrC_3NH_4^-$ (the geometrical structure is shown in Fig. S13). The presence of $IrC_3NH_4^-$ suggests the possibility of IrC^- cleaving the N–N bond in HEH.

Similar behavior as in the iridium-based interaction was observed with IrC^-. Concluding from the changes in series 4 and 5 in the mass spectra and the PE spectra, IrC^- seems to mostly form $IrC_3H_X^-$ and $IrC_3NH_X^-$ species. The mass spectra were normalized to the Ir^- peaks, and the assumption can be made that species coming from reactions of Ir^- with HEH should have similar intensities in both spectra in Fig. 2, suggesting that IrC^- has different reaction pathways with HEH than Ir^-. Using iridium carbide instead of or in combination with pure iridium might be an effective way to lower the costs for monopropellant catalyst by using less of the rare iridium for the same amount of catalyst or increasing the capability of the catalyst.

4. Conclusion

The gas phase study of the reaction of the iridium anion and HEH showed that the iridium anion can bond to different atoms in HEH. In this process, multiple bonds are broken with the extreme case where Ir^- can basically strip the carbon or nitrogen atoms of all other atoms. Cleavage of the N–N bond is supported by the theoretical data, the mass spectra and different photoelectron spectra. These reaction pathways also explain the observed products found in other studies such as hydrazine and ammonia, by breaking the N–C bond and the N–N bond in HEH, while providing hydrogen from breaking bonds at other points at the molecule. Ammonia for example could be formed, by breaking the N–N bond in HEH and releasing NH_2 which reacts with a hydrogen. This gives more insight in the actual mechanism of catalytic reactivity of HEH and might help to find out more about the hydrazine combustion by indicating that the N–N bond is broken in a reaction that is close to the combustion of hydrazine on an iridium-based catalyst.

Funding

This (experimental) material is based on work supported by the Air Force Office of Scientific Research (AFOSR) under grant number FA9550-19-1-0077 (K.H.B.). The theoretical studies were supported in part by high-performance computer time and resources from the DoD High Performance Computing Modernization Program (J.A.B.) S.D.C. thanks the Air Force Office of Scientific Research (AFOSR) under Grant FA9300-06-C-0023 for support of this work.

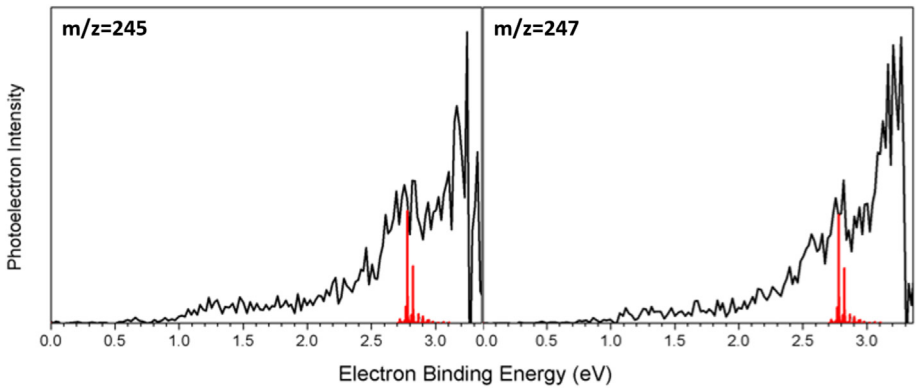

Fig. 7. Photoelectron spectra of the masses $m/z = 245$ and 247 with the theoretical spectra of $IrC_3NH_4^-$.

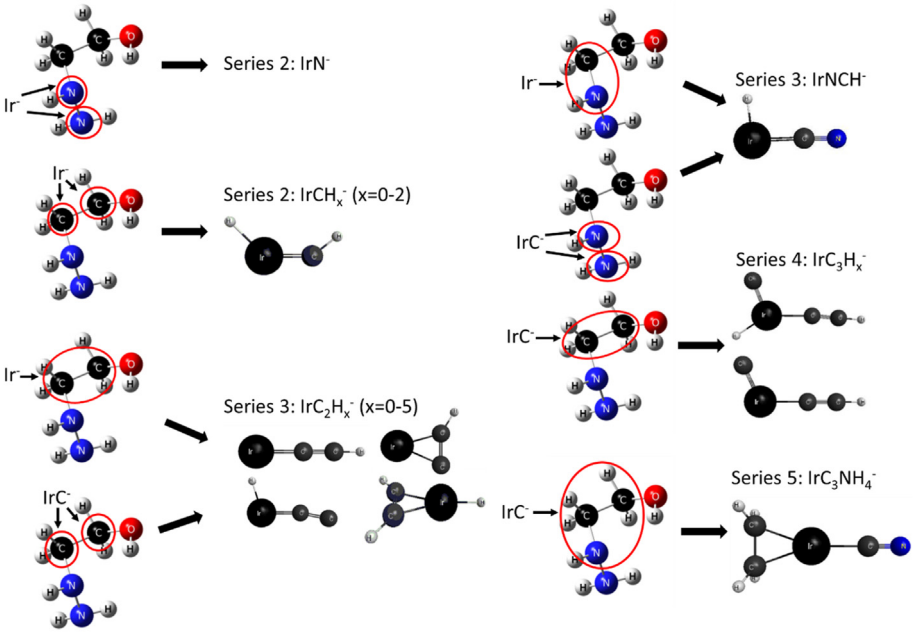

Fig. 8. Summary of Ir^-/IrC^- + HEH reactions that were confirmed by theoretical and experimental photoelectron spectra. The series corresponds to the mass spectrum in Fig. 2. The circle shows where the molecule is being attacked.

Author contributions

M.B. and T.C. completed the experimental photoelectron study. J.A.B., and S.D.C. performed the theoretical study. K.H.B, J.A.B., S.D.C and G.G. conceived of and supervised the work.

Data and materials availability

All data is available in the main text or the supplementary materials. All reasonable requests for materials will be fulfilled.

Disclaimer

The views expressed are those of the authors and do not necessarily reflect the official policy or position of the Department of the Air Force, the Department of Defense, or the U.S. government.

Declaration of competing interest

The authors declare that they have no known competing financial interests or personal relationships that could have appeared to influence the work reported in this paper.

Appendix A. Supplementary data

Supplementary data to this article can be found online at https://doi.org/10.1016/j.ijms.2022.116875.

References

[1] J.L. Shamshina, M. Smiglak, D.M. Drab, T.G. Parker, H.W.H. Dykes, R.D. Salvo, A.J. Reich, R.D. Rogers, Catalytic ignition of ionic liquids for propellant applications, Chem. Commun. 46 (2010) 8965–8967.
[2] R. Amrousse, T. Katsumi, N. Azuma, K. Hori, Hydroxylammonium nitrate (HAN)-Based green propellant as alternative energy resource for potential hydrazine substitution: from lab scale to pilot plant scale-up, Combust. Flame 176 (2017) 334–348.
[3] T. Katsumi, H. Kodama, T. Matsuo, H. Ogawa, N. Tsuboi, K. Hori, Combustion characteristics of a hydroxylammonium nitrate based liquid propellant. Combustion mechanism and application to thrusters, Combust. Explos. Shock Waves 45 (4) (2009) 442–453.
[4] S.D. Chambreau, D.M. Popolan-Vaida, G.L. Vaghjiani, S.R. Leone, Catalytic decomposition of hydroxylammonium nitrate ionic liquid: enhancement of NO formation, J. Phys. Chem. Lett. 8 (2017) 2126–2130.
[5] R. DiSalvo, H.W. Dykes Jr., R.D. Rogers, J. Shamshina, M. Smiglak, Ionic liquid monopropellant gas generator, U.S. Patent 8 (2014) 636–860.
[6] U. Swami, K. Senapathi, K.M. Srinivasulu, J. Desingu, A. Chowdhury, Energetic ionic liquid hydroxyethylhydrazinium nitrate as an alternative monopropellant, Combust. Flame 215 (2020) 93–102.
[7] A. Chowdhury, S.T. Thynell, Kinetics of decomposition of energetic ionic liquids, Propellants, Explos. Pyrotech. 35 (2010) 572–581.
[8] H.J. Zeng, T. Khuu, S.D. Chambreau, J.A. Boats, G.L. Vaghjiani, M.A. Johnson, J. Chem. Phys. 124 (2020) 10507–10516.
[9] J.Y. Cho, M.K. Tse, D. Holmes, R.E. Maleczka, M.R. Smith, Remarkably selective iridium catalysts for the elaboration of aromatic CH bonds, Science 295 (5553) (2002) 305–308.
[10] K.I. Fujita, Development and application of new iridium catalysts for efficient dehydrogenative reactions of organic molecules, Bull. Chem. Soc. Jpn. 92 (2) (2019) 344–351.
[11] Z.E. Clarke, P.T. Maragh, T.P. Dasgupta, D.G. Gusev, A.J. Lough, K. Abdur-Rashid, A family of active iridium catalysts for transfer hydrogenation of ketones, Organometallics 25 (17) (2006) 4113–4117.
[12] S.Y. Hong, Y. Park, Y. Hwang, Y.B. Kim, M.H. Baik, S. Chang, Selective formation of γ-lactams via C–H amidation enabled by tailored iridium catalysts, Science 359 (6379) (2018) 1016–1021.
[13] K. Foger, J.R. Anderson, Hydrocarbon reactions on supported iridium catalysts, J. Catal. 59 (3) (1979) 325–339.
[14] Y. Qiu, M. Stangier, T.H. Meyer, J.C. Oliveira, L. Ackermann, Iridium-catalyzed ;electrooxidative C– H activation by chemoselective redox-catalyst cooperation, Angew. Chem. 130 (43) (2018) 14375–14379.
[15] J.K. Hoyano, A.D. McMaster, W.A. Graham, Activation of methane by iridium complexes, J. Am. Chem. Soc. 105 (24) (1983) 7190–7191.
[16] W.J. Tenn, K.J. Young, G. Bhalla, J. Oxgaard, W.A. Goddard, R.A. Periana, CH activation with an O-donor Iridium– methoxo complex, J. Am. Chem. Soc. 127 (41) (2005) 14172–14173.
[17] Z. Huang, J. Zhou, J.F.N.–H. Hartwig, Activation of hydrazines by iridium (I). Double N– H activation to form iridium aminonitrene complexes, J. Am. Chem. Soc. 132 (33) (2010) 11458–11460.
[18] S.M. Ciborowski, R. Buszek, G. Liu, M. Blankenhorn, Z. Zhu, M.A. Marshall, R.M. Harris, T. Chiba, E.L. Collins, S. Marquez, J.A. Boatz, S.D. Chambreau, G.L. Vaghjiani, K.H. Bowen, Study of the reaction of hydroxylamine with iridium atomic and cluster Anions (n= 1–5), J. Phys. Chem. 125 (27) (2021) 5922–5932.
[19] J.P. Contour, G. Pannetier, Hydrazine decomposition over a supported iridium catalyst, J. Catal. 24 (3) (1972) 434–445.
[20] R. Vieira, D. Bastos-Netto, M.J. Ledoux, C. Pham-Huu, Hydrazine decomposition over iridium supported on carbon nanofibers composite for space applications: near actual flight conditions tests, Appl. Catal. Gen. 279 (1–2)

(2005) 35–40.
[21] B.J. Wood, H. Wise, The interaction of hydrazine with polycrystalline iridium foil, J. Catal. 39 (3) (1975) 471–480.
[22] S.M. Lang, T.M. Bernhardt, Gas phase metal cluster model systems for heterogeneous catalysis, Phys. Chem. Chem. Phys. 14 (26) (2012) 9255–9269.
[23] D.K. Böhme, H. Schwarz, Gas-phase catalysis by atomic and cluster metal ions: the ultimate single-site catalysts, Angew. Chem. Int. Ed. 44 (16) (2005) 2336–2354.
[24] S. Yin, E. Bernstein, Gas phase chemistry of neutral metal clusters: distribution, reactivity and catalysis, Int. J. Mass Spectrom. 321 (2012) 49–65.
[25] M. Schlangen, H. Schwarz, Effects of ligands, cluster size, and charge state in gas-phase catalysis: a happy marriage of experimental and computational studies, Catal. Lett. 142 (11) (2012) 1265–1278.
[26] B.C. Sweeny, S.G. Ard, A.A. Viggiano, N.S. Shuman, Reaction of mass-selected, thermalized $V_nO_m^+$ clusters with CCl_4, J. Phys. Chem. 123 (2019) 4817–4824.
[27] X.N. Li, X.P. Zou, S.G. He, Metal-mediated catalysis in the gas phase: a review, Chin. J. Catal. 38 (9) (2017) 1515–1527.
[28] A.J. Richard, G.N. Khairallah, Gas phase ion chemistry of transition metal clusters: production, reactivity, and catalysis, J. Cluster Sci. 15 (3) (2004) 331–363.
[29] Y. Gong, M. Zhou, L. Andrews, Spectroscopic and theoretical studies of transition metal oxides and dioxygen complexes, Chem. Rev. 109 (12) (2009) 6765–6808.
[30] K.R. Asmis, Structure characterization of metal oxide clusters by vibrational spectroscopy: possibilities and prospects, Phys. Chem. Chem. Phys. 14 (26) (2012) 9270–9281.
[31] X.L. Ding, X.N. Wu, Y.X. Zhao, S.G. He, C–H bond activation by oxygen-centered radicals over atomic clusters, Accounts Chem. Res. 45 (3) (2012) 382–390.
[32] S. Zhou, J. Li, M. Schlangen, H. Schwarz, Bond activation by metal–carbene complexes in the gas phase, Accounts Chem. Res. 49 (3) (2016) 494–502.
[33] J. Roithova, D. Schroder, Selective activation of alkanes by gas-phase metal ions, Chem. Rev. 110 (2) (2010) 1170–1211.
[34] A.A. Esparza, S.D. Chambreau, G.L. Vaghjiani, E. Shafirovich, Two-stage decomposition of 2-hydroxyethylhydrazinium nitrate (HEHN), Combust. Flame 220 (2020) 1–6.
[35] J.C. Howard, G. Cever, A.B. Neill, P.H. Weil, The thermal decomposition of 2-hydrazinoethanol and 1-hydrazino-2-propanol, J. Org. Chem. 26 (4) (1961) 1082–1083.
[36] X. Zhang, G. Liu, G. Ganteför, K.H. Bowen, A.N. Alexandrova, PtZnH5-, A s-Aromatic Cluster, J. Phys. Chem. Lett. 5 (2014) 1596–1601.
[37] J. Ho, K.M. Ervin, W.C. Lineberger, Photoelectron spectroscopy of metal cluster Anions: Cu-n, Ag-n, and Au-n, J. Chem. Phys. 93 (1990) 6987.
[38] J.-D. Chai, M. Head-Gordon, Systematic optimization of long-range corrected hybrid density functionals, J. Chem. Phys. 128 (2008), 084106.
[39] J.-D. Chai, M. Head-Gordon, Long-range corrected hybrid density functionals with damped Atom–Atom dispersion corrections, Phys. Chem. Chem. Phys. 10 (2008) 6615–6620.
[40] F. Weigend, R. Ahlrichs, Balanced basis sets of split valence, triple zeta valence and quadruple zeta valence quality for H to Rn: design and assessment of accuracy, Phys. Chem. Chem. Phys. 7 (2005) 3297–3305.
[41] D. Rappoport, F. Furche, Property-optimized Gaussian basis sets for molecular response calculations, J. Chem. Phys. 133 (2010) 134105.
[42] D. Andrae, U. Häußermann, M. Dolg, H. Stoll, H. Preuß, Energy-adjusted ab initio pseudopotentials for the second and third row transition elements, Theor. Chim. Acta 77 (1990) 123–141.
[43] The def2-TZVPPD basis set and stuttgart pseudopotentials were downloaded from the Basis Set Exchange (BSE) website. https://www.basissetexchange.org/.
[44] B.P. Pritchard, D. Altarawy, B. Didier, T.D. Gibson, T.L. Windus, A new basis set exchange: an open, up-to-date resource for the molecular sciences community, J. Chem. Inf. Model. 59 (2019) 4814–4820.
[45] D. Feller, The role of databases in support of computational chemistry calculations, J. Comput. Chem. 17 (1996) 1571–1586.
[46] K.L. Schuchardt, B.T. Didier, T. Elsethagen, L. Sun, V. Gurumoorthi, J. Chase, J. Li, T.L. Windus, Basis set exchange: a community database for computational sciences, J. Chem. Inf. Model. 47 (2007) 1045–1052.
[47] D.A. McQuarrie, Statistical Mechanics, Harper & Row, New York, 1975.
[48] The zero point energy scale factor of 0.975 used here is the value recommended for ωB97x-d/def2-TZVP; see "computational thermochemistry: scale factor databases and scale factors for vibrational frequencies obtained from electronic model chemistries," I. M. Alecu, J. Zheng, Y. Zhao, and D. G. Truhlar, J. Chem. Theor. Comput. 6, 2872-2887 2010.
[49] M.W. Schmidt, K.K. Baldridge, J.A. Boatz, S.T. Elbert, M.S. Gordon, J.H. Jensen, S. Koseki, N. Matsunaga, K.A. Nguyen, S.J. Su, et al., General atomic and molecular electronic structure system, J. Comput. Chem. 14 (1993) 1347–1363.
[50] M.S. Gordon, M.W. Schmidt, Advances in electronic structure theory: GAMESS a decade later, in: Theory and Applications of Computational Chemistry, Elsevier, 2005, pp. 1167–1189.
[51] Gozem, S.; Krylov, A. I. The EzSpectra suite: an easy-to-use toolkit for spectroscopy modeling. Wiley interdiscip. Rev.: Comput. Mol. Sci. 2021, No. e1546.
[52] Samer Gozem, Pawel Wojcik, Vadim Mozhayskiy, and anna Krylov. http://iopenshell.usc.edu/downloads.
[53] F. Duschinsky, Zur Deutung der Elektronenspektren mehratomiger Moleküle. I. Über das Franck–Condon Prinzip., *Acta Physicochim*. URSS 7, 551-566 1937.
[54] J. Wang, X. Sun, Z. Wu, Theoretical investigation of 5d-metal monocarbides, J. Cluster Sci. 18 (1) (2007) 333–344.